Transport in Porous Media (2006) 65: 31–51
DOI 10.1007/s11242-005-6092-5

Estimation of Dynamic Relative Permeability and Capillary Pressure from Countercurrent Imbibition Experiments

J. M. SCHEMBRE and A. R. KOVSCEK*
Department of Petroleum Engineering, Green Earth Science Bldg, Stanford University, Stanford, CA 94305-2220, USA

(Received: 13 September 2004; accepted in final form: 2 November 2005)

Abstract. Direct laboratory measurements of *in situ* water-phase saturation history are used to estimate relative permeability and capillary pressure functions. The magnitude of so-called nonequilibrium effects during spontaneous imbibition is quantified and, if significant, these effects are incorporated within the estimation technique. The primary constraint employed is that curves must increase or decrease monotonically; otherwise, no predetermined functionality is assumed. The technique is demonstrated using water saturation profile histories obtained for diatomite (a low-permeability and high-porosity rock). Results indicate that nonequilibrium effects detected at laboratory scale in low-permeability rocks influence the estimation of unsteady-state relative permeability and capillary pressure.

Key words: countercurrent imbibition, relative permeability, capillary pressure, nonequilibrium effects.

Nomenclature

b	degree of B-spline.
$B_{j,p}(u)$	B-spline basis function of degree p.
c_i	control point.
C_i^j	control point for k_{rw}, k_{rnw}, P_c.
D	diffusion constant
E	objective function.
k_b	Boltzmann's constant.
k	absolute permeability.
k_p	relative permeability of phase p.
J	Leverett function.
m	number of interior knots in B-Splines.
N	degree of freedom in B-spline definition.
N_T	Markov chain length.
P_c	capillary pressure.
S_i^j	control point for S_w.

* Author for correspondence: e-mail: kovscek@pangea.stanford.edu

S_p saturation for phase p.
t time.
w_i component of the knot vector, W, in spline definition.
x position of saturations.

Greek Symbols

α_{red} reduction factor.
η effective aqueous phase saturation.
ϕ porosity.
ρ density.
ϱ vector of unknowns in simulated annealing.
λ_p mobility of phase p.
μ fluid viscosity.
Θ temperature used in simulated annealing.
τ relaxation time.

Subscripts/Superscripts

c capillary pressure.
calc calculated.
meas measured.
nw non wetting.
w wetting.

1. Introduction

The laboratory methods used to measure relative permeability functions are grouped into centrifuge, steady-state, and unsteady techniques (Honarpour *et al.*, 1986; Rose, 1987). Each group offers advantages and disadvantages as thorough reviews elsewhere discuss (Loomis and Crowell, 1962; Hirasaki *et al.*, 1995). A variety of concerns persist with the centrifuge method. For instance, viscous forces are replaced by centrifugal forces and this replacement may affect unsteady state displacement processes that are rate dependent (Ali, 1997). Also, information at low water saturation cannot be gained from centrifuge production data at low mobility ratio (Hirasaki *et al.*, 1995).

Steady-state methods require both phases to approach local equilibrium. This requirement results in time-consuming measurements for low-permeability porous media because it is laborious to reach multiple steady states that are free of capillary-end effects (Firoozabadi and Aziz, 1991; Kamath *et al.*, 1995). Capillary forces have a significant effect on multiphase flow, saturation distribution as a function of time, and recovery history in low-permeability rocks.

Application of conventional unsteady-state techniques to low permeability rocks does not appear to be generally acceptable (Akin and Kovscek, 1999). Other unsteady methods infer relative permeability by history-matching experimental data such as pressure drop and/or multiphase fluid production, for example MacMillan (1987), Jennings *et al.*

(1988), Kohhedee (1994), and Reynolds *et al.* (2004). Such methods assume, typically, that relative permeability and capillary pressure curves follow some predetermined functionality. For instance, a Corey-type power-law function (Corey, 1954) is assumed, commonly, for relative permeability. Such functionality does not describe multiphase flow in some low-permeability systems (Schembre and Kovscek, 2003). Moreover, obtaining accurate experimental data for history-matching of relative permeability curves is difficult. One major challenge is to measure accurately the pressure gradient (Schembre and Kovscek, 2003). We overcome this difficulty by developing a method that uses simulated annealing optimization to estimate simultaneously capillary pressure and relative permeability from aqueous-phase saturation profiles during spontaneous imbibition as measured by X-ray computerized tomography (CT) scanning. Such estimates, while nonunique, are significantly constrained by the measured *in situ* saturation histories.

The technique proposed acknowledges that the assumption of instantaneous local equilibrium may be inappropriate for interpretation of some spontaneous imbibition laboratory data such as those reported by Zhou *et al.* (2003) and Le Guen and Kovscek, (2006) . Nonequilibrium effects are interpreted according to the model developed by Barenblatt *et al.* (Barenblatt, 1971; Barenblatt and Gilman, 1987; Barenblatt *et al.*, 2003; Silin and Patzek, 2004). We note also that alternate approaches to interpretation of time-dependent behavior exist (Hassanizadeh *et al.*, 2002). The primary feature of Barenblatt's model employed here is that the redistribution of phases in the pore space, as the porous medium fills with water, is not instantaneous, but requires a certain period of time. As a result, two-phase relative permeability and capillary pressure are not solely functions of the instantaneous water saturation *when* the redistribution time is significant. Rather, they are process-dependent quantities with values different from those measured at the same water saturation in steady-state flow experiments. To our knowledge, this work represents the first attempt to combine Barenblatt's model of spontaneous countercurrent imbibition with measurements of *in situ* phase saturation history to extract multiphase flow properties. We return to the details of implementation later.

This paper has three main parts. First, we summarize the experimental data set employed and describe some peculiarities of diatomite. Second, we present the main methodology for application of the technique to saturation profiles measured experimentally. Here, nonequilibrium effects are considered and we show a practical approach to incorporate them in the determination of relative permeability and capillary pressure. In a sense, we show how to interpret unsteady-state laboratory data to infer corresponding steady-state relative permeability curves. Finally, results are presented and contrasts made between incorporation and neglect of rate processes during immiscible flow.

Table I. Core properties and test conditions

Reference	Wetting fluid	Nonwetting fluid	ϕ%	k (%md)	T (° C)	Resolution Pixel
Zhou *et al.* (2001)	Water	Air	70	7	22	271
Le Guen and Kovscek (2006)	Water	Decane	77	7.9	22	220

2. Experimental Data

We employ a data set comprised of water saturation profile histories collected in our laboratory (Zhou *et al.*, 2001; Le Guen and Kovscek, 2006). These data resulted from two-phase, countercurrent, spontaneous water imbibition into rock. Recall that water imbibition, as opposed to drainage, is a critical mechanism of secondary oil recovery from fractured oil reservoirs.

The porous medium was diatomite (Grefco Quarry, Lompoc, CA). Diatomite is composed of the remains of microscopic shells of diatoms (single shell plankton). Typically, porosity ranges from 50%–70% and permeability varies from 0.1 to 10 md (Akin *et al.*, 2000). These quarry samples are also known to be water wet (Akin and Kovscek, 1999). Cores were cut in a direction parallel to the bedding plane and were 2.5 cm in diameter and 9.5 cm long. The nonwetting fluids were air and n-decane. In one case, the core contained both decane and water initially ($S_{wi} = 5\%$), and in the other, the core was filled with air ($S_{wi} = 0\%$). In both cases, the wetting phase is water. Table I summarizes properties of the cores and the information source.

After the initial saturation was established, water was pumped through an endcap while all other surfaces of the core were sealed. The flow channels in the endcap have large dimension and the pressure drop is correspondingly small. The oil recovered by countercurrent imbibition was removed by water flowing through the endcap. Saturation profiles as a function of time were measured using X-ray computed tomography (CT) (Akin and Kovscek, 2003). Spatial resolution was 0.25 mm by 0.25 mm by 10 mm. Image processing of the CT data provided values of water saturation (fraction of the pore volume occupied by water) along the core length. Thus, consecutive images taken during the experiment provided the position of any saturation value as the imbibition process progressed. Visual inspection of CT images allowed simple selection of experiments that presented uniform one-dimensional flow (Zhou *et al.*, 2001). Three-dimensional saturation data was reduced to one-dimensional profiles by averaging all data across the width of the core at a particular

axial location. The column labeled "pixel resolution" in Table I is the number of saturation measurements along the flow direction after averaging. The experimental procedure and equipment are described in detail by Zhou *et al.* (2001), Tang Kovscek (2004) and Le Guen and Kovscek (2006).

Two independent analyses have concluded that these experiments demonstrate detectable nonequilibrium effects (Silin and Patzek, 2004; Le Guen and Kovscek, 2006). Silin and Patzek (2004) extended the model of Barenblatt *et al.* (Barenblatt, 1971; Barenblatt and Gilman, 1987; Barenblatt *et al.*, 2003) significantly. They assume that relaxation time is not a constant, but is, in fact, a function of water saturation. As a demonstration of the utility of their model, they matched experimental oil recovery data resulting from the countercurrent imbibition of water as reported by (Zhou *et al.*, 2003). More recently, Le Guen and Kovscek, (2006) conducted further experiments and analyzed the resulting saturation profiles using a similarity transform method. Essentially, a plot of aqueous phase saturation versus the similarity variable $x/t^{0.5}$ collapses all saturation profiles to a single curve for all times *when* the relaxation time is zero or negligible. Le Guen and Kovscek (2006) found significant deviation among experimental and numerical local-equilibrium based results. The nonequilibrium effects inferred in this data set may, or may not, be negligible at large scale, but their presence must certainly be acknowledged during the laboratory estimation of rock-fluid properties, that ultimately become input for numerical modeling.

3. Method

The objective of the estimation method is to match experimental and numerically calculated water saturation profiles to obtain two-phase relative permeability and capillary pressure functions. Thus, the difference between the position measured, x^{meas}, and the position calculated by the forward model, x^{calc}, for each *in situ* saturation value as a function of time, is minimized. The objective function, E, is written

$$E = \frac{\left[\sum_{i=0}^{N_{\text{prof}}} \sum_{j=1}^{N_{\text{sat}}} \left(x^{\text{calc}}(S_{w_j}, t_i) - x^{\text{meas}}(S_{w_j}, t_i)\right)^2\right]^{1/2}}{N_{\text{sat}} N_{\text{prof}}}, \tag{1}$$

where the product $N_{\text{sat}} N_{\text{prof}}$ is the number of measured aqueous phase saturations to be matched. E is minimized using simulated annealing (Kirkpatrick *et al.*, 1983). Details follow to aid those who may choose to implement the method.

The simulated annealing algorithm associates a "temperature", Θ, with the state of a model or system. The energetically optimal configuration is found by repeatedly trying to alter the state of the system. Transitions

that lower the energy state are automatically accepted. If the transition has larger energy, the value of Θ in Equation (2) defines the probability of acceptance of this undesirable move

$$P_{\mathrm{r}}(\Delta E) = \exp\left(-\frac{\Delta E}{k_{\mathrm{b}}\Theta}\right), \tag{2}$$

where k_{b} is the Boltzman constant and ΔE is the change of energy of the suggested move. This property allows the system to escape from local minima. A simulated annealing algorithm is completely defined upon specification of the initial temperature of the system, a rule for determining the number of iterations, N_T, that the temperature remains constant, a rule for determining the temperature decrement, and a termination criterion. In our study, the rule to decrease the temperature is

$$\Theta_{\mathrm{new}} = \alpha_{\mathrm{red}}\Theta_{\mathrm{old}}, \tag{3}$$

where α_{red} is the reduction factor (Ouenes *et al.*, 1994; Godman, 1997). After trial and error, we chose $\alpha_{\mathrm{red}} = 0.3$, $N_T = 300$, and the termination criterion was a tolerance $< 10^{-5}$.

3.1. B-SPLINES

Relative permeability curves for low permeability rocks do not necessarily have any functional form (Schembre and Kovscek, 2003). Thus, we do not limit the shape of the relative permeability and capillary pressure relations to some predetermined function. We employ B-spline expansions that have been shown to represent successfully a diversity of functions (Kerig and Waston, 1986; Watson *et al.*, 1988; Yang and Waston, 1991; Kulkarni and Datta-Gupta, 1999).

Given $N+1$ control points $c_0, c_1, \ldots, c_N$ and a knot vector $W = w_0, w_1, \ldots, w_m$, the B-spline curve, C, is defined as

$$C(w) = \sum_{j=o}^{N} c_j B_{j,b}(w), \tag{4}$$

where $B_{j,b}(w)'s$ are B-spline basis functions of degree m. The degree of freedom, N, is given by the sum of the order of the spline and the number of interior knots. The degree b is defined as $b = m - N - 1$.

The basis functions are defined as

$$B_{j,0}(w) = \begin{cases} 1 & \text{if } w_i \leqslant w < w_{i+1} \quad \text{and} \quad w_i < w_{i+1}, \\ 0 & \text{otherwise,} \end{cases} \tag{5}$$

$$B_{j,b}(w) = \frac{w - w_j}{w_{j+b} - w_b} B_{j,b-1}(w) + \frac{w_{j+b+1} - w}{w_{j+b+1} - w_{j+1}} B_{j+1,b-1}(w). \tag{6}$$

For relative permeability and capillary pressure functions, we write

$$k_{ri}(w) = \sum_{j=1}^{N_i} C_j^i B_{j,b}^m(w), \tag{7}$$

$$P_c(w) = \sum_{j=1}^{N_c} C_j^c B_{j,b}^m(w), \tag{8}$$

where $i = w, \mathrm{nw}, c$ represents wetting phase, nonwetting phase, and capillary pressure, respectively. The constraints on C_j^i read: for $i = w C_j^i < C_{j+1}^i$; for $i = \mathrm{nw}$ and $i = c$, $C_j^i > C_{j+1}^i$. The B-spline partition needs to be specified. In general, 5–6 control points are used. The location of the relative permeability and capillary pressure values, calculated by Equations (7) and (8), respectively, are provided by

$$S_w^i(w) = \sum_{j=1}^{N_i} S_j^i B_{j,b}^m(w), \tag{9}$$

$$S_w^c(w) = \sum_{j=1}^{N_i} S_j^c B_{j,b}^m(w). \tag{10}$$

These coefficients were fixed throughout the optimization procedure. Equation (1) is optimized by changing the coefficients $C_{1\cdots N_w}^w$, $C_{1\cdots N_{\mathrm{nw}}}^{\mathrm{nw}}$ and $C_{1\cdots N_c}^c$. Moving the coefficients changes the local shape of the curve.

3.2. GENERAL FORMULATION

As a preliminary step, we locate the position of the measured saturation, $x^{\mathrm{meas}}(S_{w_j}, t_i)$ from X-ray CT images. We use the commercial finite-difference based simulator ECLIPSE (GeoQuest, 2001) as the forward model, to compute the position of each saturation x^{calc}. The core is modeled using Cartesian block-centered coordinates with 1001 cells in the z-direction. A grid refinement study of 201, 501, and 1001 cells indicated minimal numerical dispersion with 1001 cells. The first cell has fracture properties. It is assigned a pore-volume multiplier and it is 100% water saturated at all times to emulate the experimental water source. The remaining cells are assigned the corresponding rock and oil properties of the experiment. The initial time step is set to 10^{-5}s and time-step control is automatic within the simulator. The solutions are only allowed to proceed if converged at the previous time step.

Simulated annealing finds the spline coefficients that minimize the objective function, Equation (1). To validate the method, we used two, synthetic, water–oil countercurrent cases with zero initial water saturation. These cases assumed local equilibrium. The phase viscosities were characteristic of water and crude oil at high temperature. The details and specifics of the validations are found elsewhere (Schembre, 2004). The greatest relative error was obtained for large and small S_w, with a total average relative error of 5%. This error is less than experimental error.

3.3. INCORPORATION OF NONEQUILIBRIUM EFFECTS

This section lays out the methodology for incorporation of nonequilibrium effects while estimating relative permeability and capillary pressure. The equation for Darcy velocity during countercurrent imbibition is (Zhou *et al.*, 2001).

$$u_w = \frac{\lambda_w \lambda_{\mathrm{nw}}}{\lambda_t} \frac{\partial P_c}{\partial x} \tag{11}$$

and

$$\lambda_i = \frac{k_{ri}}{\mu_i}. \tag{12}$$

In the classical approach, it is assumed that $k_{\mathrm{rw}}, k_{\mathrm{rnw}}$, and P_c are solely functions of the water saturation. Based on this assumption, Equation (11) is rearranged to read

$$S_w \frac{\mathrm{d}x/\mathrm{d}t|_{S_w}}{\partial S_w/\partial x|_{S_w}} = \frac{-k k_{\mathrm{rnw}}}{\phi \mu_{\mathrm{nw}}} f(S_w) = D(S_w), \tag{13}$$

where

$$f(S_w) = \frac{1}{1 + \frac{k_{\mathrm{rnw}} \mu_w}{k_{\mathrm{rw}} \mu_{\mathrm{nw}}}} \tag{14}$$

and $D(S_w)$ is the hydraulic diffusivity, e.g., Reis and Cili (2000).

In strongly unsteady flows, such as capillary imbibition of a porous block, the classical model in Equation (13) seems inadequate (Barenblatt and Gilman, 1987; Barenblatt *et al.*, 2003). In these processes, flow paths rearrange as capillary pressure decreases. Therefore, a time period, τ, is required to approach local equilibrium and constant flow paths. This time is also called the redistribution time (Silin and Patzek, 2004). To evaluate the relative permeability and capillary functions accounting for this redistribution time, an effective water saturation, η, is defined. It is assumed that the effective and actual saturations are related through the rate of change of the actual saturation (Barenblatt, 1971; Barenblatt and Gilman, 1987).

A kinetic equation characterizes this relationship. Dimensional analysis and linearization of this equation lead to (Barenblatt *et al.*, 2003)

$$\eta = S_w + \tau \frac{\partial S_w}{\partial t}, \tag{15}$$

where $\frac{\partial S_w}{\partial t}$ is the change of saturation with time at a particular position. All terms on the right of Equation (15) are available from our experimental data.

The redistribution time, τ, is obtained by matching the dimensionless oil production versus time data with the predictions of Equation (16) as demonstrated by Silin and Patzek (2004):

$$R(t) = V_o \left(1 - e^{\frac{t}{\tau}}\right) \sqrt{\frac{t}{\tau}}, \tag{16}$$

where V_o depends on the characteristics of the core and fluids. Thus, we minimize the difference between Equation (16) and the experimental data to obtain V_o and τ. Another simplifying assumption is that τ is constant for all saturation values.

Figure 1 illustrates schematically the difference between the steady-state water relative permeability $k_{\mathrm{rw}}(S_w)$ and the corresponding dynamic relative permeabiilty $k_{\mathrm{rw}}(\eta)$ at some particular t. One interpretation of η is that it is a saturation at a certain time ahead of the actual time. Thus, the dynamic relative permeability of water at the actual time is greater than the steady-state relative permeability evaluated at the instantaneous saturation, S_w. For small values of $\tau \frac{\partial S_w}{\partial t}$, we recover naturally the local-equilibrium result.

Because relative permeability and capillary pressure curves are assumed to be functions solely of phase saturations by the simulator, an inner loop is annexed to our algorithm that accounts for time dependence. At each

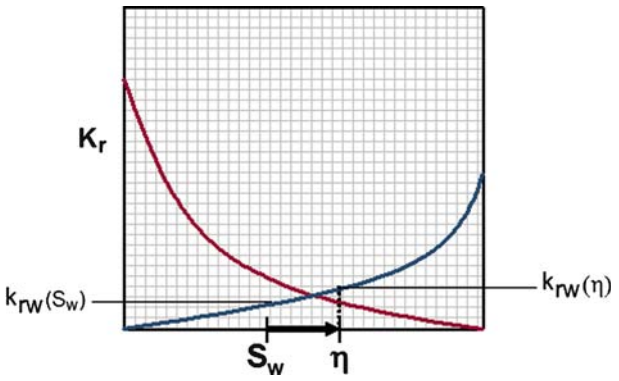

Figure 1. Relationship between steady-state water relative permeability, $k_{\mathrm{rw}}(S_w)$, and dynamic value evaluated at the effective saturation $k_{\mathrm{rw}}(\eta)$.

time step, the simulator maps the phase saturations and pressures into temporary files. It modifies the relative permeabilities and capillary pressure from the steady-state relative permeability, according to Equation (15) and performs the flow simulation for the next time step.

4. Results

Experimental data are analyzed first without consideration of nonequilibrium effects and then with incorporation of the effective saturation concept. Figures 2 and 3 summarize relative permeability and capillary pressure curves, respectively, for the water–air–diatomite system as obtained with the method described above. The broken line presents the resulting curves where nonequilibrium effects are excluded from the interpretation method. Results incorporating nonequilibrium effects are discussed shortly. Figure 4 compares the experimental and calculated wetting-phase saturation profiles as a function of time using the local-equilibrium relative permeabilities and capillary pressure relationships shown (broken lines) in Figures 2 and 3. The relative error among saturation profiles is 8% and is concentrated mainly in the saturation profiles obtained at short times such as 5 and 13 min.

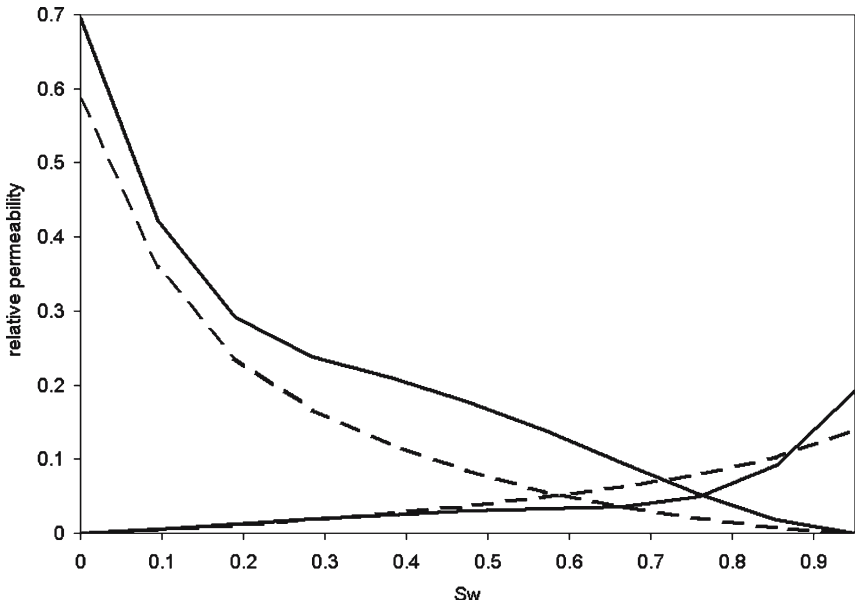

Figure 2. Relative permeability functions obtained for countercurrent imbibition performed in water–air diatomite systems. Broken lines denote nonequilibrium effects are excluded from the calculations, whereas solid lines include nonequilibrium effects.

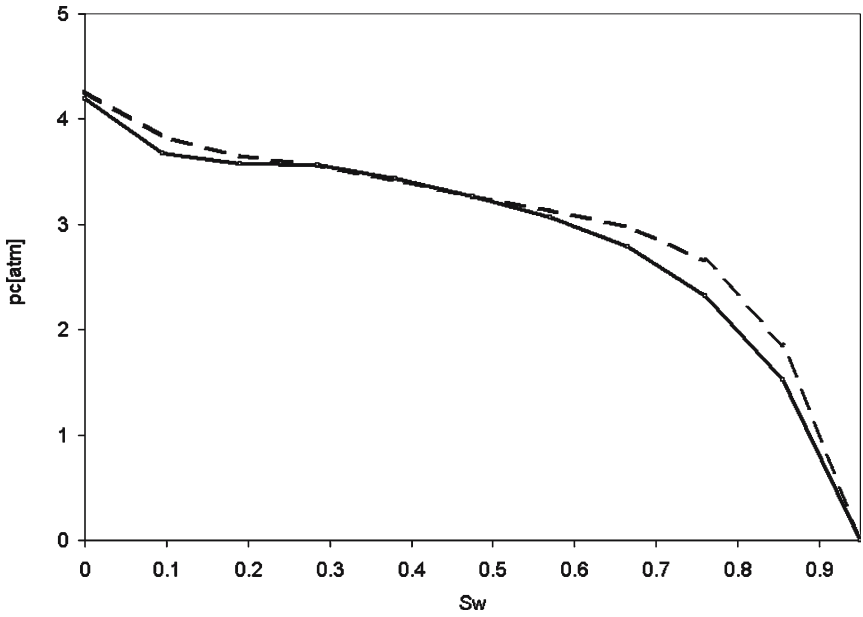

Figure 3. Capillary pressure obtained for countercurrent imbibition performed in water–air diatomite systems. Broken lines denote nonequilibrium effects are excluded from the calculations, whereas solid lines include nonequilibrium effects.

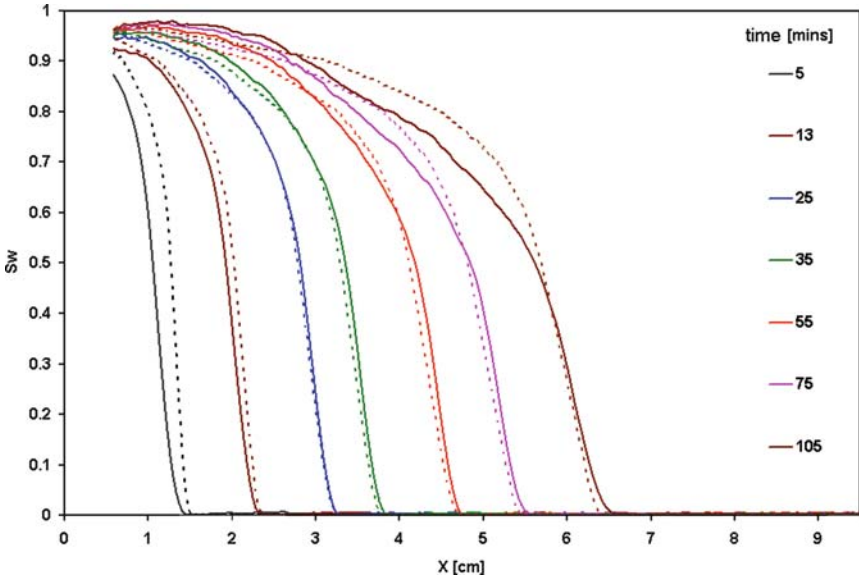

Figure 4. Water–air countercurrent imbibition: comparison of experimental water saturation profiles (solid lines) and simulation profiles (broken lines) with increasing time using the relative permeability and capillary functions in Figures 2 and 3 that do not include nonequilibrium effects. Relative error is 8%.

The procedure was repeated for the system water–decane–diatomite. The resulting curves appear in Figures 5 and 6. In this case the relative error between experimental and computed S_w profiles is 14%. Most of the error is due to the unusual saturation profile shown at earlier times, mostly in the high water saturation range, Figure 7. This affects the displacement profiles at later times.

Comparison of Figures 2 and 3 with Figures 5 and 6 reveals that the nonwetting phase saturation remaining after spontaneous imbibition varies with the composition of the nonwetting phase. In the case of air, the residual saturation is less than 5%, whereas with decane it is about 25%. In both systems, the relative permeability of water at the residual nonwetting phase saturation is less than roughly 0.2. This result is indicative of the largest pores being filled with nonwetting phase and it is consistent with a water-wet system. Initial water saturations are low, or zero, for each system. Nevertheless, the relative permeability of the nonwetting phase is not 1 at the initial water saturation. A small increase in the wetting phase saturation appears to reduce the relative permeability to the nonwetting phase significantly consistent with the concept of significant interference of phases during multiphase flow (Honarpour *et al.*, 1986).

In short, both Figures 4 and 7 show that water saturation profiles present a mismatch in the front shape and location at early times, in order to match the experimental values at later times. This observation has been reported by other authors in experiments with countercurrent imbibition (Parsons and Chaney, 1964; Zhang *et al.*, 1996; Leventis *et al.*, 2000). This

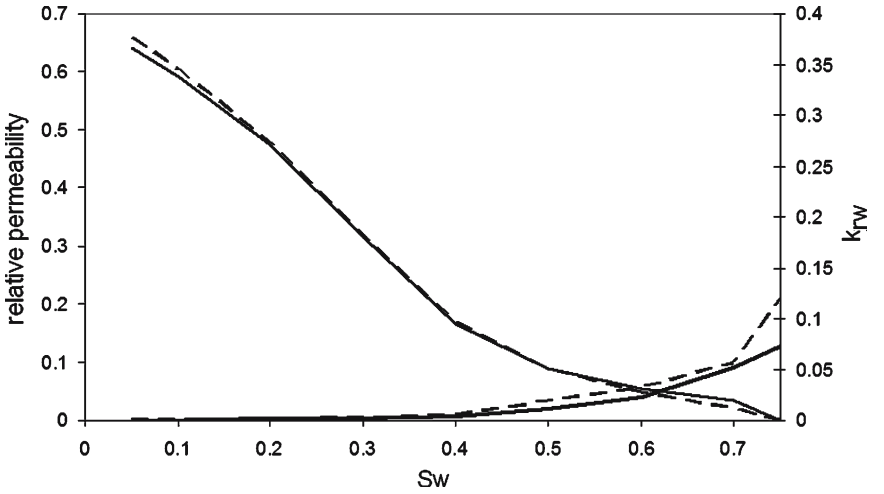

Figure 5. Relative permeability functions obtained for countercurrent imbibition performed in water–decane–diatomite systems. Broken lines do not include nonequilibrium effects, whereas solid lines include nonequilibrium effects.

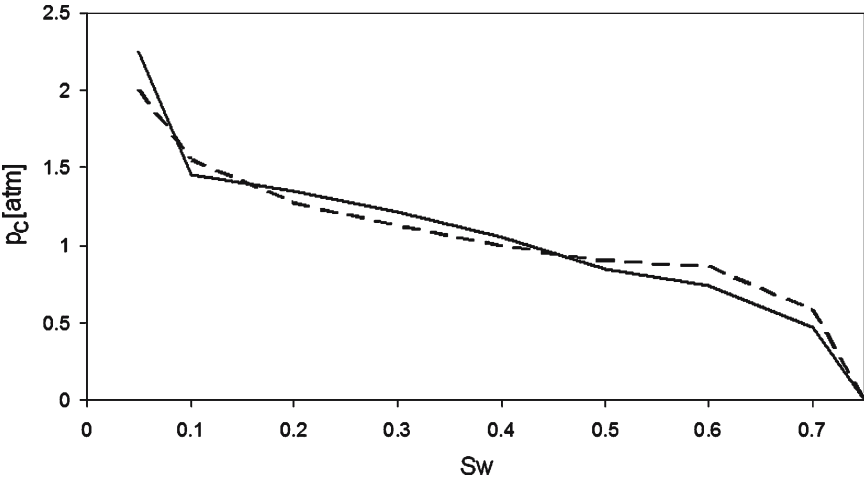

Figure 6. Capillary pressure obtained for countercurrent imbibition performed in water–decane–diatomite system. Broken lines do not include nonequilibrium effects, whereas solid lines include nonequilibrium effects.

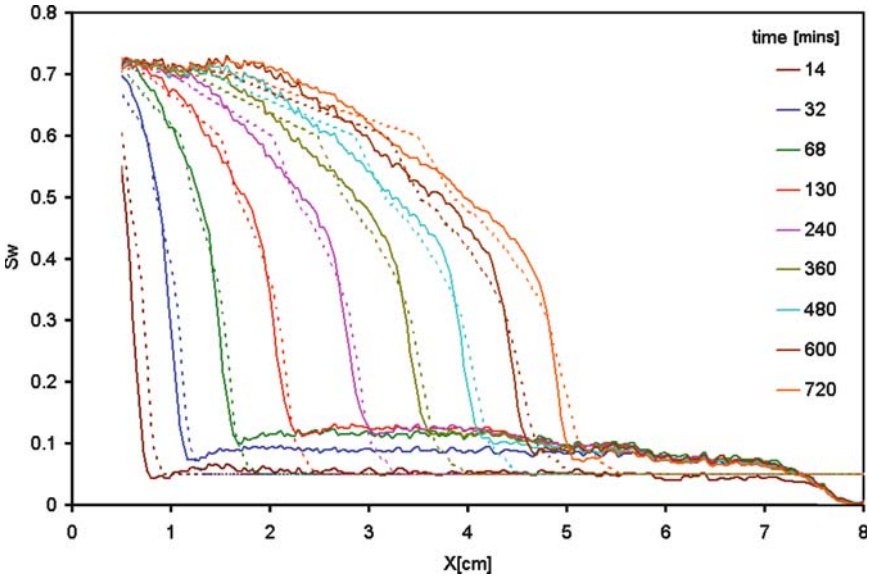

Figure 7. Water–Decane countercurrent imbibition: comparison of experimental water saturation profiles (solid lines) and simulation profiles (broken lines) with increasing time using the relative permeability and capillary functions in Figures 5 and 6 that do not include nonequilibrium effects. Relative error is 14%.

pattern is regarded as consequence of nonequilibrium effects (Silin and Patzek, 2004, Le Guen and Kovseck, 2006).

4.1. INCORPORATION OF NONEQUILIBRIUM EFFECTS

All parameters needed to estimate steady-state relative permeability from dynamic data are available in the experimental data. In this section, we assess the implications of nonequilibrium effects on the interpretation of experiments.

Table II lists the redistribution time, τ, and characteristic volume, V_o, obtained for the two countercurrent experiments under analysis. The values of τ are less than 160 s for both systems. This redistribution time appears to be small compared to the time required to complete the experiment. Yet, a plot of η versus S_w, for the water–air case (Figure 8), with the least τ, reveals remarkable differences between the measured water saturation and corresponding effective saturation as a function of time. The transformation from S_w to η space takes place according to Equation (15). Differences are greatest at early times and decrease as time progresses and the system approaches capillary equilibrium. The time dependence displayed in Figure 8 implies that hydraulic diffusivity (Equation (13)) is indeed a function of water saturation and time.

Next, the estimation technique incorporating process dependent saturation is applied to both relative permeability and capillary pressure curves. Figures 9 and 10 illustrate how relative permeability and capillary pressure curves evolve with time for the water–air countercurrent case. To obtain each curve, S_w measurements are transformed to η and relative permeability and capillary pressure are evaluated as outlined in Figure 1. The solid black line, in Figure 9, is the inferred steady-state relative permeability where S_w and η are identical. Dashed lines indicate the values at different times. Notice that the major deviations from the inferred steady-state relationship are at the earlier times, as expected.

Figure 11 summarizes the saturation profile history for the water–air system and accounts for dynamic relative permeability and capillary pressure in the calculated results. Dynamic relative permeability and capillary pressure functions for the water–air case are represented by solid lines in Figures 2 and 3. Water saturation profiles match to a greater degree than previously. In

Table II. τ and V_o values

System	τ sec	V_o
Water/air	87.0	0.058
Decane/water	155	0.056

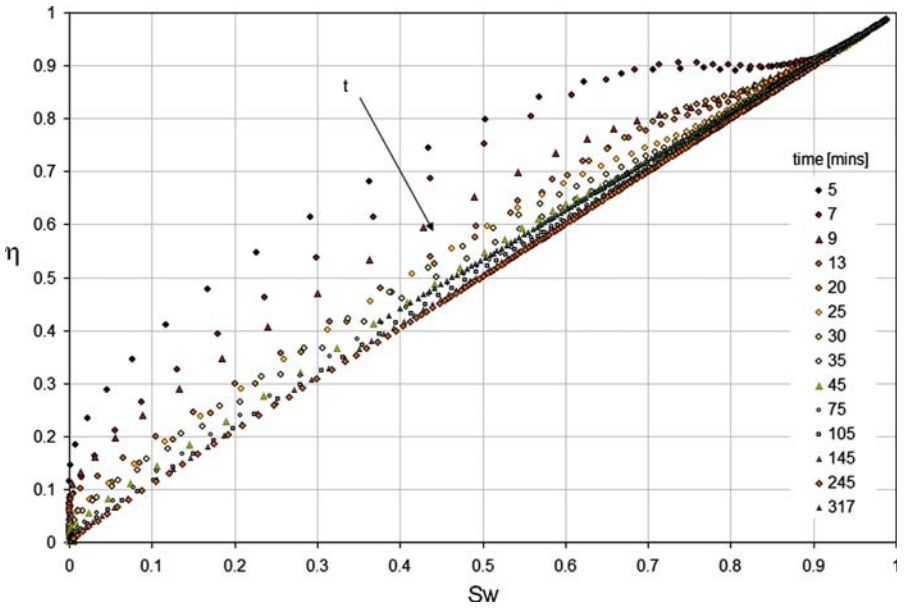

Figure 8. Crossplot of effective saturation, η, versus measured water saturation, S_w, as a function of time: water–air–diatomite system. The arrow indicates increasing time.

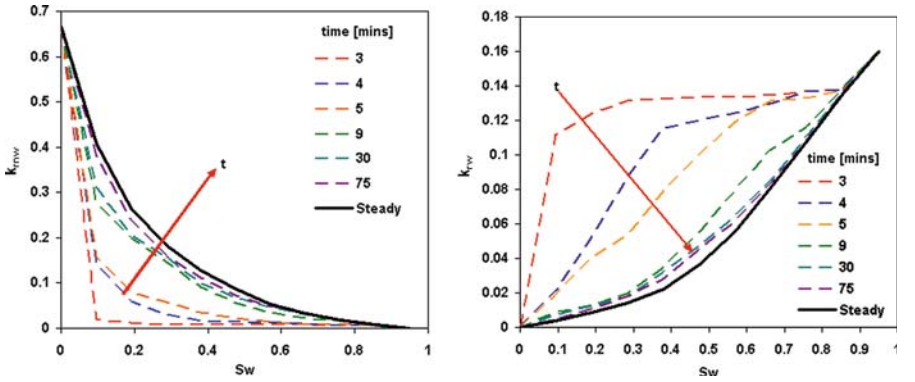

Figure 9. Time dependent relative permeability curves. Different curves denote relative permeability curves used for each simulation step before local equilibrium is attained. The arrow indicates increasing time.

this case, the relative error is 5%, compared to 8% when we do not consider nonequilibrium effects (Figure 4). Figures 2 and 3 compare relative permeabilities and capillary pressure functions for the water–air case, respectively. Again, the broken lines represent the curves estimated without accounting for nonequilibrium effects. The solid lines represent the curves estimated including the nonequilibrium effects in the calculations.

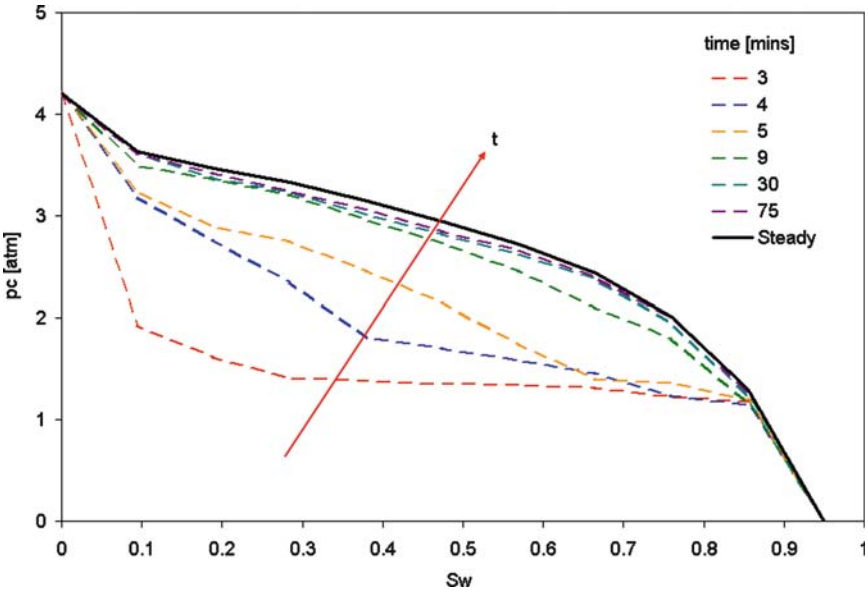

Figure 10. Time dependent capillary pressure curves. Different curves denote capillary pressure curves used for each simulation step before local equilibrium is attained. The arrow indicates increasing time.

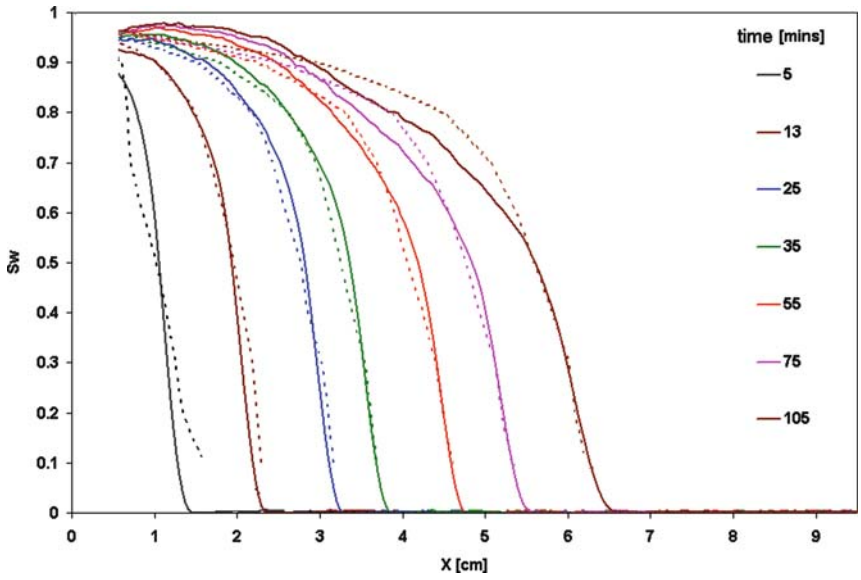

Figure 11. Water–air–diatomite countercurrent imbibition including dynamic relative permeability and capillary pressure. Comparison of experimental water saturation profiles (solid lines) and simulation profiles (broken lines). Relative error is 5%.

Next, the technique was applied to oil–water spontaneous countercurrent imbibition data. Figure 12 shows the resulting saturation profiles using the relative permeability and capillary pressure functions shown in Figures 5 and 6 (solid lines). The error was reduced in this case from 14% to 8%. Comparison of the resulting relative permeability (Figures 2 and 5) and capillary pressure (Figures 3 and 6) curves indicates a noticeable shift in both functions with the inclusion of nonequilibrium effects. Further, the shift is in the same direction for both systems.

5. Discussion

Overall, we judge that the incorporation of nonequilibrium effects in the interpretation of laboratory data that exhibit relatively small redistribution times has improved the quality and reliability of the curves obtained. Certainly, the respective errors between measured and calculated saturation profiles of 5% and 8% is on par with the experimental measurement error.

The fluid-rock systems analyzed here employ clean fluids, are relatively ideal, and have small τ. We have applied the estimation technique to viscous, heavy-oil systems in field core (Schembre *et al.*, 2005) at a variety of temperatures. At a temperature of 120 °C, oil viscosity is about 15 mPa s and τ is roughly, 3000 s. Temperature was elevated because thermally

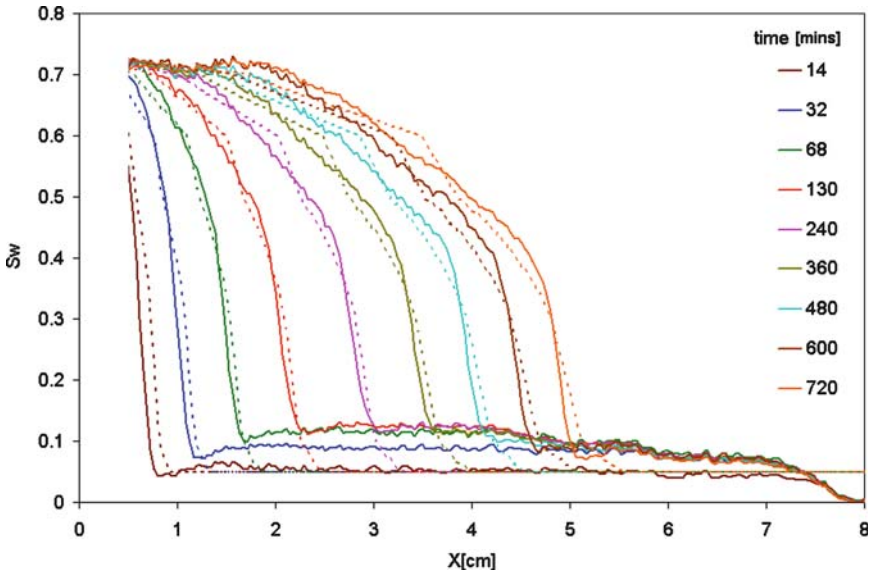

Figure 12. Countercurrent imbibition in the water–decane–diatomite system including dynamic relative permeability and capillary pressure. Comparison of experimental water saturation profiles (solid lines) and simulation profiles (broken lines). Relative error is 8%.

enhanced oil recovery was under evaluation. This data proved difficult to interpret without consideration of nonequilibrium effects, but using the technique outlined here, realistic steady-state relative permeability curves were inferred from experiments at a variety of temperatures. Additionally, a shift in rock wettability with temperature was measured and related to changes in the shape of the relative permeability curves.

The inclusion of nonequilibrium effects when determining relative permeability and capillary pressure relationships has repercussion when comparing the curves after normalizing the water saturation using the initial and nonwetting phase residual saturations (Honarpour *et al.*, 1986). When nonequilibrium effects are included and plotted versus normalized saturation (Schembre, 2004), both relative permeability relationships are nearly the same. This is the expected result for clean systems where the nonwetting phase is relatively inviscid. On the other hand, the curves differ significantly when nonequilibrium effects are disregarded. Note that the same rock is used for both experiments. On the contrary, the capillary pressure curves, hence Leverett-J function are more distanced from each other with the inclusion of nonequilibrium effects (Schembre, 2004). A possible explanation is that the initial dynamics of large saturation values greatly impacts the shape of the P_c curve.

6. Conclusions

Nonequilibrium effects, detected at laboratory scale influence the estimation of relative permeability and capillary pressure functions. As these constitutive relationships are essential input for numerical simulation, neglecting nonequilibrium effects while analyzing unsteady laboratory data ultimately leads to inaccurate assessment of multiphase flow properties.

Two countercurrent, spontaneous imbibition experiments were used to illustrate an interpretive technique. Results were compared with calculations that assume instantaneous equilibrium. Without the inclusion of nonequilibrium effects, the relative permeability and capillary pressure curves obtained do not yield reproduction of the measured *in situ* saturation history within experimental error. On the other hand, inclusion of nonequilibrium effects reduces the relative estimation error 38% in the water–air case and 48% in the water–decane case, with respect to cases that did not incorporate nonequilibrium effects. Computed and measured saturation histories then agreed within experimental error. The functions obtained are consistent, generally, with previous results for these formations.

Specific conclusions include:

1. Unsteady-state, laboratory, measurement techniques for relative permeability and capillary pressure should quantify and account for nonequilibrium effects.

2. As such, imaging of the distribution of phases *in situ* is vital to obtain accurate relationships from unsteady-state techniques.
3. Experimental data provide all the information necessary to estimate the redistribution time as well as relative permeability and capillary pressure.
4. For the diatomite rock employed here, relative permeability and capillary pressure relationships do not exhibit commonly assumed power-law functionalities.
5. Water relative permeability endpoint ranges between 0.06 and 0.21. The crossover of oil and water relative permeability is located in a bracket of high water saturations, denoting water wettability of these particular diatomite rocks. Inclusion of nonequilibrium shifts curves such that greater water wetness is indicated.

Acknowledgements

We thank L. Jia and S. Le Guen for providing the experimental data used in this study. Also, we thank D. Silin for comments, suggestions, and encouragement during the various stages of this work. This work was prepared with the support of the U.S. Department of Energy, under Award No.DE-FC26-00BC15311. Any opinions, findings, conclusions, or recommendation expressed herein are those of the author and do not necessarily reflect the views of the DOE. Additionally, the support of the Stanford University Petroleum Research Institute (SUPRI-A) Industrial Affiliates is gratefully acknowledged.

References

Akin, S. and Kovscek, A. R.: 1999, Imbibition studies of low-permeability porous media. SPE 54590, *Proceedings of the Western Regional Meeting,* Anchorage, Alaska, May 26–29.

Akin, S., Schembre, J. M., Bhat, S. K. and Kovscek, A. R.: 2000, Spontaneous imbibition characteristics of diatomite, *J. Petrol. Sci. Eng.* **25**, 149–165.

Akin, S. and Kovscek, A. R.: 2003, Computed tomography in petroleum engineering research, in: F. Mees, Swennen R., M. Van Geet and P. Jacobs (eds), *Application of X-ray Computed Tomography in the Geosciences*, Geological Society, London, Special Publications **215**, 23–38.

Ali, J. K.: 1997, Development in measurement and interpretation techniques in coreflood tests to determine relative permeabilities, SPE 39016. Presented at the Fifth Latin American and Caribbean Petroleum Engineering Conference and Exhibition Rio de Janiero, Brazil, 30 Aug–3 Sept.

Barenblatt, G.: 1971, Filtration of two nonmixing fluids in a homogeneous porous medium, *Soviet Academy Izvestia. Mech. Gas Fluids* **5**, 857–864.

Barenblatt, G. I. and Gilman, A. A.: 1987, A mathematical model of non-equilibrium countercurrent capillary imbibition, *Eng. Phys. J.* **52**(3), 46–61.

Barenblatt, G. I., Patzek, T. W. and Silin, D. B.: 2003, The mathematical model of non-equilibrium effects in water–oil displacements, *Soc. Petrol. Eng. J.* **8**(4), 409–416.

Corey, A. T.: 1954, The interrelation between gas and oil relative permeabilities, *Producer's Monthly* **19**, 38–41.

Firoozabadi, A. and Aziz, K.: 1988, Relative permeabilities from centrifuge data, *J. Canad. Petrol. Technol.* **30**(5), 33–42.

GeoQuest.: 2001, *ECLIPSE Reference Manual 2001A*, Schlumberger.

Godman, D. E.: 1997, Simulated annealing applied to a problem in combinatorial optimization. Technical report, Department of Computer Science, University of Illinois at Urbana-Champaign, Illinois.

Hassanizadeh, S. M., Celia, M. A. and Dahle, H. K.: 2002, Dynamic effect in the capillary pressure-saturation relationship and its impacts on unsaturated flow, *Vadose Zone J.* **1**, 38–57.

Hirasaki, G. J., Rohan, J. H. and Dudley, J. W.: 1995, Interpretation of oil–water relative permeabilities from centrifuge experiments, *SPE Adv. Technol. Series* **3**(1), 66.

Honarpour, M., Koederitz, L. and Harvey, A. H.: 1986, *Relative Permeability of Petroleum Reservoirs*, CRC Press, Boca Raton, Florida.

Jennings, J. W., McGregor, D. S. and Morse, R. A.: 1988, Simultaneous determination of capillary pressure and relative permeability by automatic history matching, *Soc. Pet. Eng. Form. Eval.* **3**(2), 322–328.

Kamath, J., deZabala, E. F. and Boyer, R. E.: 1995, Water/oil relative permeability endpoints of intermediate wet, low permeability rocks, *Soc. Petrol. Eng. Formation Eva.* **10**(1), 4–10.

Kerig, P. D. and Watson, A. T.: 1986, Relative permeability estimation from displacement experiments: an error analysis, *Soc. Petrol. Engs. Reservoir Eng.* Mar, 175.

Kirkpatrick, S., Gelatt, C. D. and Vecchi, M. P.: 1983, Optimization by simulated annealing, *Science* **220**(4598), 671–680.

Kohhedee, J. A.: 1994, Simultaneous determination of capillary pressure and relative permeability of a displaced phase, SPE 28827. in: *Proceedings of the European Petroleum Conference*, London, U.K., 25–27 Oct.

Kulkarni, K. N. and Datta-Gupta, A.: 1999, Estimating relative permeability from production data: A streamline approach. SPE 56751, *Proceedings of SPE Annual Technical Conference and Exhibition,* Houston, Texas, 3–6 Oct.

Le Guen, S. S. and Kovscek, A. R.: (in press), Non equilibrium effects during spontaneous imbibition, *Transp. Porous Media.*

Leventis, A., Verganelakis, D. A., Halse, M. R., Webber, J. B. and Strange, J. H.: 2000, Capillary imbibition and pore characterisation in cement pastes, *Transp. Porous Media.* **39**, 143–157.

Loomis, A. G. and Crowell, D. C.: 1962, Relative permeability studies: Gas–oil and water–oil systems, *Bull. USBM.* **599**.

MacMillan, D. J.: 1987, Automatic history matching of laboratory corefloods to obtain relative permeability curves, *Soc. Pet. Eng. Res Eng.* **2** (1), 85–91.

Ouenes, A., Bhagavan, S., Bunge, P. H. and Travis, B. J.: 1994, Aplication of simulated annealing and other global optimization methods to reservoir description: Myths and realities. SPE 28415, *Proceedings of the SPE 69th Annual Technical Conference and Exhibition,* New Orleans, LA, 25–28 Sept.

Parsons, R. W. and Chaney, P. R.: 1964, Imbibition model studies on water–wet carbonate rocks, *SPE J.* **26** (Mar), 26–34.

Patzek, T. W.: 2001, Verification of a complete pore network simulator of drainage and imbibition, *SPE J.* **6**(2), 144–156.

Reis, J. and Cil, M.: 2000, Analytical models for capillary imbibition: Multidimensional matrix blocks, *In situ* **24**(1), 79–106.

Reynolds, A. C., Li, R. and Oliver, D. S.: 2004, Simultaneous estimation of absolute and relative permeability by automatic history matching of three-phase flow production data, *J. Can. Petrol. Technol.* **43**(3), 37–46.

Rose, W.: 1987, Relative permeability, in *Handbook of Petroleum Engineering* (2nd edn), Chapter 26.

Schembre, J. M.: 2004, Temperature, surface forces, wettability and their relationship to relative permeability of porous media, Ph.D. Thesis, Stanford University.

Schembre, J. M. and Kovscek, A. R.: 2003, A technique for measuring two-phase relative permeability in porous media via X-ray CT measurements, *J. Petrol. Sci. Eng.* **39**, 159–170.

Schembre, J. M., Tang, G.-Q., and Kovscek, A. R.: 2005, Effect of temperature on relative permeability for heavy-oil diatomite reservoirs, SPE 93831. Presented at the SPE Western Regional Meeting Irvine, CA, 30 Mar–1 Apr.

Silin, D. B. and Patzek, T. W.: 2003, On Barenblatts model of spontaneous countercurrent imbibition, *Transp. Porous Media* **54(3)**, 297–322.

Strenski, P. N.: 1987, Optimal annealing schedules. Technical report, RC 12923, (#58001). Computer Sciences, Stanford University, California.

Tang, G. and Kovscek, A. R.: 2004, An experimental investigation of the effect of temperature on recovery of heavy-oil from diatomite. *Soc. Petrol. Eng. J.* **9(2)**, 163.

Watson, A. T., Richmond, P. C., Kerig, P. D. and T. T. M.: 1988, A regression-based method for estimating relative permeability from displacement experiments. *Soc. Petrol. Eng. Reservoir Eng.*, Aug, 953–958.

Yang, P. H. and Watson, A. T.: 1991, A bayesian methodology for estimating relative permeability curves. *SPE Reservoir Eng.*, May, 259–265.

Zhang, X., Morrow, N. R. and Ma, S.: 1996, Experimental verification of a modified scaling group for spontaneous imbibition, *Soci. Petrol. Eng. Reservoir Eng.* Nov, 280–285.

Zhou, D., Jia, L. Kamath, J. and Kovscek, A. R.: 2002, Scaling of Counter-current imbibition processes in low permeability porous media. *J. Petrol. Sci. Eng.* **33**, 61–74.